Proceedings of the ASME 2023
International Mechanical Engineering Congress and Exposition
GT2023
June 26–30, 2023, Boston, MA

GT2023-103410

PART-LOAD BEHAVIOR AND START UP PROCEDURE OF A REVERSE RANKINE HIGH TEMPERATURE HEAT PUMP WITH WATER AS ITS WORKING MEDIUM

Maximilian Kriese*, **Steffen Klöppel**, **Nico Setzepfand**, **Robert Schaffrath**, **Eberhard Nicke**

German Aerospace Center, Institute of Low-Carbon Industrial Processes

ABSTRACT

In recent years, the issue of sustainability, especially in terms of resource utilization, has become increasingly prominent. In contrast, even today a large part of the process heat required in industry is obtained by burning fossil fuels. In order to meet this demand sustainably, the development of high-temperature heat pumps has steadily increased in recent years. Nowadays, heat pump systems are mostly commercially available up to a temperature level of 90 °C. Even taking into account the few demonstration pilot plants up to temperature levels of 160 °C, there is a certain gap up to 200°C which would by needed for a variety of industrial applications. To overcome this gap and their experimental evidence the DLR has designed the pilot plant ZiRa. In this paper, the construction of the plant and the steady state simulation results are presented. Based on the reversed Rankine cycle the pilot plant is able to lift the temperature from 120 °C at source to 200 °C at the sink with a COP of 3.4. This is achieved by a three-stage compression. The compressors are described by their respective performance maps, which are used to investigate the operating range of the plant by varying the source temperature between 100 °C and 130 °C. In addition, the performance of the system was investigated in relation to the compressor part-load range. It has been shown that even with small changes in the respective compressor speed, the performance varies in terms of discharge pressure and sink temperature. Finally, the start-up procedure of the pilot plant is described.

Keywords: High Temperature Heat Pump, Part-load Operation, Reverse Rankine Cycle, Process Simulation

NOMENCLATURE

Greek Letters

η	efficiency
κ	heat capacity ratio
Π	pressure ratio

Symbols

A	heat transfer area
c_p	specific heat capacity
E_{in}	exergy flow at inlet on primary side of respective heat exchanger
E_{out}	exergy flow at outlet on primary side of respective heat exchanger
k	heat transfer coefficient
$\dot{m}$	massflow
n	compressor speed
p	pressure
P	power
T_t	total temperature
$\dot{W}$	work
$\dot{Q}$	heat flow
$\dot{Q}_{rel}$	released heat in inter- and after-coolers as well as condenser

Abbrevation

CFD	computational fluid dynamics
COP	coefficient of performance
DLR	German Aerospace Center
HPC	high pressure compressor
HTHP	high temperature heat pump
HTSC	high temperature secondary cycle
KVS	flow coefficient
LPC	low pressure compressor
LTSC	low temperature secondary cycle
MPC	medium pressure compressor
ZiRa	Zittau Rankine Cycle Heat Pump

Subscripts

0	inlet
2	outlet
I	state 1
II	state 2
comp	variable for the respective compressor

*Corresponding author: Maximilian.Kriese@dlr.de

Drive	variable for the electric drive of each compressor
Gearbox	variable for the gearbox of each compressor
Imp	impeller
red	reduced
s	saturated steam condition
Sink	location of heat release
Source	location of absorption
sucked	state of the sucked water vapor upstream of the compressor
superheated	state of superheated steam
total	sum of all work input

1. INTRODUCTION

The European Union (EU) aims for climate neutrality by 2050. This goal can be realistically achieved by considerable efforts in the coming years and decades, since every sector needs to be decarbonized. Besides the more prominent electricity generation and transport sector, a large fraction of the greenhouse gas emissions can be attributed to the industry, in particular to the generation of process heat. In 2019, the worldwide process heating amounted to 19 % of the overall energy demand [1]. The generation of process heat can be decarbonized by using renewable energy for direct electric heating, synthetic fuels (e.g. hydrogen, methanol) or high temperature heat pumps. The latter are especially efficient with COPs (ratio of invested electricity to provided heat) of about 3 to 8, depending on the available heat source and the required heat sink temperature.

Heat pumps are commercially available up to 90 °C, while demonstration plants reach up to 165 °C [2]. However, there is a significant demand of process heat up to 200 °C in the food, paper, chemical and refinery industry [3][4]. However, right now there is a certain reluctance in the industrial sector to use the high-temperature heat pump technology, which is according to [2] due to three factors:

- a knowledge gap in the development of high temperature heat pumps,
- experience with natural refrigerants as working fluid and
- the availability of suitable components.

To address these factors, a pilot plant is designed and constructed which allows to demonstrate a heat pump with a sink temperature of up to 200 °C. As its working media water respectively water vapor is used for mainly three reasons. First, the long-used fluorocarbons are besides the climate harmful impact not viable working fluids at such high temperatures. In comparison, water vapor has no impact on the environment (global warming potential of 0) and has a comparatively high enthalpy of vaporization as well as an high critical point (374 °C and 221 bar(a)). The second reason is the almost infinite availability. And last, most industrial plants depend on steam networks.

The latter factor mentioned above is mainly related to the compression technology, which is one of the main challenges for the commercial application of this type of heat pump. In this article, the authors report on the overall design of the pilot plant as well as the design of the compressors and the integration into the circuit with a focus on start-up and partial load operation.

1.1 Reversed Rankine Cycle

The basic working principle of an HTHP based on the reversed Rankine cycle is shown in Figure 1. Starting from point 1, superheated water vapor is sucked in by the compressor. The super-heat is defined as follows:

$$T_{\text{superheat}} = T_{\text{sucked}} - T(p_{\text{s}}). \tag{1}$$

After the compression process, the water vapor reaches a temperature and pressure maximum at point 2. Subsequently, the water vapor enters the condenser. Where it is condensed and the condensation heat is supplied to an external consumer as useful heat. Next, the water vapor is expanded through a throttle to the initial pressure level, into the wet steam area. Finally, the two-phase working medium is evaporated, so that the initial state is reached.

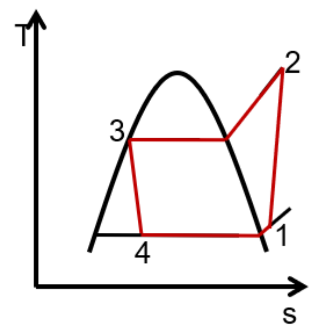

FIGURE 1: REVERSED RANKINE PROCESS IN THE T-S DIAGRAM

1.2 Prototype Pilot ZiRa

At the Institute for Low Carbon industrial processes of the DLR are currently two pilot plants in construction, which should address two of the three above mentioned challenges, the knowledge gap and the usage of natural refrigerants in high temperature heat pumps. The first one is the pilot plant CoBra which is based on the reverse Brayton cycle [5], [6] and uses air as working fluid. The second pilot plant ZiRa, which is the scope of this work, is a HTHP based on the reverse Rankine process that uses deionized water as its working medium. Its purpose is to gather experience in the operation of water-based HTHP and demonstrate the technology. The latest development state is picture in Figure 2. The pilot plant ZiRa aims to achieve in a first step a condensation temperature of 200 °C (see point 8 in Figure 2) using a three-stage compression system. The pilot plant can be divided into three different subsystems. There is the primary cycle (displayed in red and dark blue in Figure 2), in which the heat pump process takes place. The other two cycles are the high (HTSC - displayed in green) and the low temperature secondary cycle (LTSC- displayed in purple), respectively.

The primary cycle consists of three compressor stages (including a bypass), a condenser, a throttle and an evaporator. The total pressure difference in the primary cycle correlates with the possible temperature lift. In addition, the respective compressor efficiency correlates with the general performance of the system. Therefore, their design is of particular importance. Available heat

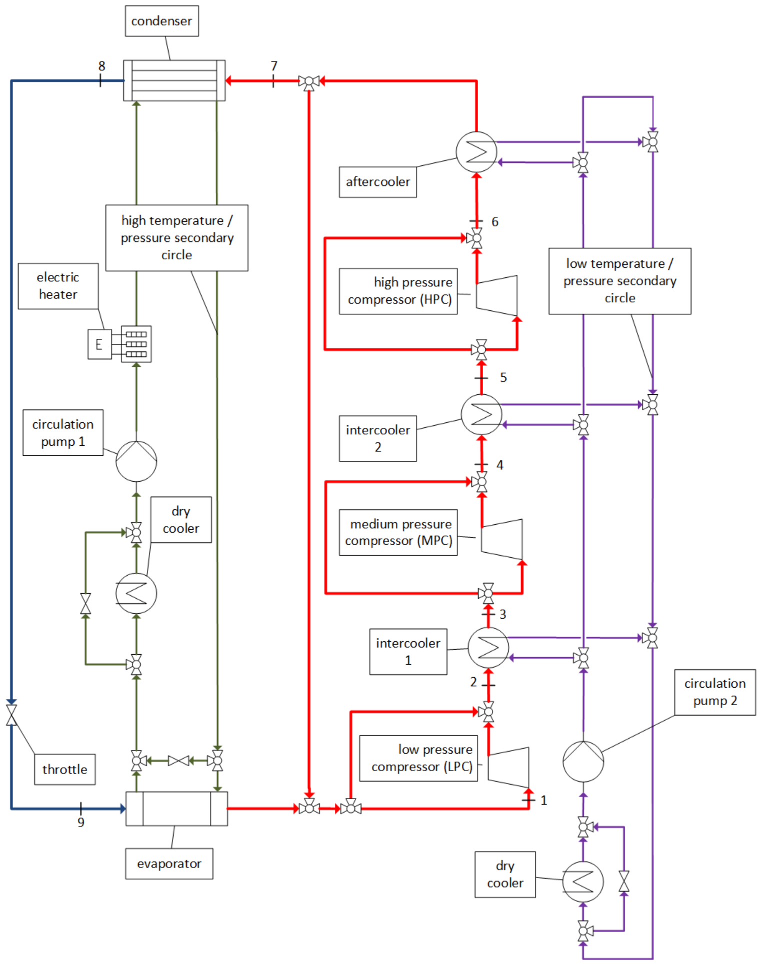

FIGURE 2: SCHEMATIC DESIGN OF THE PILOT ZIRA

pump systems use positive displacement machines, i.e. piston or screw compressors, which have poorer efficiency compared to turbo compressors. Another disadvantage is the comparatively larger space requirement and the limited operating range, based on the maximum achievable temperature level. In addition, oil lubrication is required, which can contaminate the working medium, which is why oil separators must be used [7]. For these reasons, turbo compressors are used for the pilot plant ZiRa. Nevertheless, turbo compressors, respectively centrifugal compressors have some challenges such like the rotor-dynamic behavior or the sealing as well. Latter can be crucial with respect of the compressor lifetime because of some potential leakage flow to the bearing, respectively the lubrication system. If water vapor gets through the sealing into the bearing, condensation will take place. The water will contaminate the oil, which will decrease its lubricity. That can potentially cause a component failure.

According to [8], [9] and [10] the pressure ratio for a steam compressor can reach values up to $\Pi = 3.5$. Meroni et al. [11] have shown that an individuell design, respectively preliminary design has to be carried out for a specific refrigerant to match the specfic needs for the heat pump system. In addition, because the low molecular weight of water, which is why high blade tip speeds will be necessary to achieve reasonable pressure ratios and temperature lift per stage, an optimization of the compressor is required. Such a design process for a steam compressors is shown by Schaffrath et al. [12]. The stage pressure ratio achieved showed comparatively poor efficiency, which is why a three-stage compression was implemented in the design of the pilot ZiRa. Those three compression stages have a combined nominal power consumption of around 150 kW. Each compressor is connected to a gear box and an electric drive. Furthermore, each stage is equipped with a bypass, which will be used for the start-up procedure. The bypass in the connection upstream of the condenser and downstream of the evaporator ensures that the working medium will be in its liquid form when exiting condenser, also during off-design operations.

The HTSC connects the evaporator with the condenser and serves two purposes. On the one hand the HTSC transfers the generated heat between the condenser and the evaporator to save installation space and simultaneously reduce the operational cost of the pilot system. The gained heat can not be completely used for the evaporation, that is why the dry cooler is implemented so that the remaining enthalpy is dissipated to the environment. On the other hand the HTSC is used for the start up, which is why the electric heater is implemented. Latter will heat up the water circulating in the HTSC to the operating temperature in the evaporator. Therefore, the pressure kept at 32 bar(a), ensuring the refrigerant to remain in its liquid state. (pressure maintaining system - not displayed in Figure 2). In the design condition, the HTSC operates between two temperature levels: at 190 °C between the condenser and the evaporator and at 140 °C downstream of the evaporator and upstream of the condenser. A low-temperature secondary cycle (LTSC) was implemented to separate the large heat flows in the evaporator/condenser from the smaller heat flows in the intercoolers and thus, simplify the construction of the respective heat exchanger and the control concept for the entire plant. This means that in an industrial application, all heat could be transfered from the primary cycle into the secondary cycle. The flow in each intercooler respectively in the aftercooler can be regulated, aiming for a 10 K degree of superheating for the steam at its outlet in the primary cycle [13]. Therefore, the LTSC is designed for a pressure of 6 bar(a) and 50 °C.

2. MODEL DESCRIPTION

The part load behavior is derived from a steady state simulation model of the pilot plant ZiRa. For the simulation the software Ebsilon Professional [14] was used. The thermodynamic properties of the fluid are calculated based on the IAPWS-IF 97 equations [15]. For both the design case as well as for the off-design case the evaluation of the performance of the pilot plant ZiRa is carried out by the coefficient of performance (COP), which is calculated as follows:

$$\mathrm{COP} = \frac{\sum \dot{Q}_{\mathrm{Sink}}}{\sum \frac{\dot{W}}{\eta_{\mathrm{Drive}}\,\eta_{\mathrm{Gearbox}}\,\eta_{Imp.}}} \tag{2}$$

The numerator represents the sum of all heat flows which could possibly cover a potential industrial demand. In the presented pilot plant, these consist of the heat transferred to the cooling water in the intercoolers (LTSC) and the heat delivered to the high-pressure secondary system (HTSC) in the condenser of the heat pump. The denominator contains the sum of electric power used to drive the three compressors including the gearbox and drive loses. It is assumed that both, the electric drive and the gearbox have an efficiency of 95 %. In the following sections, the modeling process of the part-load characteristics for the main components of the HTHP will be described.

In addition, the theoretical COP can be calculated by adding the exergy differences on the primary side of each heat exchanger, including the evaporator, for which the sum is negative. This gives the theoretical input power that is needed for upgrading the heat to the respective temperatures. By dividing the released heat by said value, the theoretical COP can be found:

$$COP_{th} = \frac{\sum Q_{rel}}{\sum E_{in} - E_{out}} \tag{3}$$

Two things should be mentioned nevertheless: Firstly, this calculation assumes that there is a matching need for the heat at the respective temperatures levels (sliding temperature profile in the after coolers). Secondly, the finite temperature differences in the heat exchangers are neglected.

2.1 The compression system of the HTHP and its model

The compression system is the most crucial subsystem in the presented HTHP, because its efficiency has a direct influence on the on-design COP and the operating range (off design) of the heat pump. In the pilot plant ZiRa, only centrifugal compressors are considered, due to their high efficiency, their scalability and their capability to withstand harsh operational conditions (high temperature and pressure). A commercially available compression system from the automotive industry has been chosen for the low-pressure compressor. The medium-pressure compressor is an aerodynamically adapted and structurally redesigned version of this system. The high-pressure compressor stage is a new design in terms of aerodynamics, structural mechanics, rotor dynamics, sealing and bearing. This development will be done in cooperation with an industrial partner. The boundary conditions for both independently designed compressors stages are presented in table 1. The three compressor stages are characterized by the respective performance map, as presented in Figure 3. This includes (MPC and HPC) the respective design point for the self-designed compressors, which is highlighted by a yellow star.

The performance maps shown here as well as further maps presented in this paper were determined according to the design conditions. The manufacturer ASA Compressor GmbH has experimentally determined the performance map of the low-pressure compressor (LPC) for air under International Standard Atmosphere inlet conditions (15 °C and 1013.25 hPa). The performance map for the medium (MPC) and the high-pressure compressor (HPC) were obtained by numerical flow simulations. Those simulations were carried out assuming an adiabatic system. The computational procedure for this approach can be found in the work of Schaffrath et.al [12]. Due to the adiabatic boundary condition, the computed pressure ratios are reduced in the simulations by 15 %. The efficiency is also reduced by an offset of 5 %. These assumptions are based on empirical data obtained from earlier investigations through the DLR.

TABLE 1: DESIGN PARAMETERS OF THE COMPRESSOR STAGES

Design parameter	MPC	HPC
Inlet temperature [°C]	151.7	178.3
Inlet pressure [bar(a)]	3.8	7.6
Required power [kW]	45	50
Rotational speed [min^{-1}]	100.000	70.000
Isentropic efficiency [%]	67	64.5

2.2 Heat exchangers, pipes and valves

Based on the design, heat exchangers are characterized by the kA-values. Hereby, k is the heat transfer coefficient and A is heat exchange area. The part-load behavior is characterized to the changes of the heat transfer coefficient. For this purpose, a linear dependency of the heat transfer coefficient based on the ratio of the current mass flow to the design mass flow is assumed. The pipes are modeled by specifying diameter [16] and length. These values are used to determine the pressure losses in the design and in the part-load case. The tubes are assumed to be adiabatic. Finally, valves and fittings are accounted in the model as additional sources of pressure loss. The pressure drop variation as a function of the flow rate is determined using the respective KVS value of the valves.

2.3 Simulation methodology and boundary conditions

Essentially, there are two boundary conditions that limit the operation of the pilot plant. The operating range is influenced by the performance map of each compressor stage and by the maximum transferable power of the gearbox (50 KW continuous load for the LPC and MPC). As already described, the performance maps are implemented in the simulation model so that an error message would appear if the surge/choke limit is exceeded. The maximum possible mass flow rate is estimated assuming an isentropic change of state (see Equation 4).

$$P_{comp} = \dot{m}*\Delta h = \dot{m}*c_p*T_{t0}*[(\frac{p_2}{p_0})^{\frac{\kappa-1}{\kappa}} - 1] \tag{4}$$

The operating range of the plant is mainly evaluated based on the compressor performance maps. Generally speaking, in this context the understanding of part load means a reduced speed of the compressors. However, in the scope of this paper part-load is referred to as the change in the inlet condition. This is necessary for two reasons: On the one hand, even in continuous industrial processes, there are fluctuations that cause changes in the inlet conditions. On the other hand, the individual industrial processes differ fundamentally in terms of the process heat requirement and the available source temperature. Therefore, the compressors must be able to operate under these different entry states, which cause a displacement in the operating range for each compressor. The displacement is calculated based on the Mach similarity (see [17] and [18]). Accordingly, two operating states are similar or comparable to one another if their Mach number distribution is the same. In addition, the definition of the Mach number is expanded to include the ideal gas equation and the continuity equation.

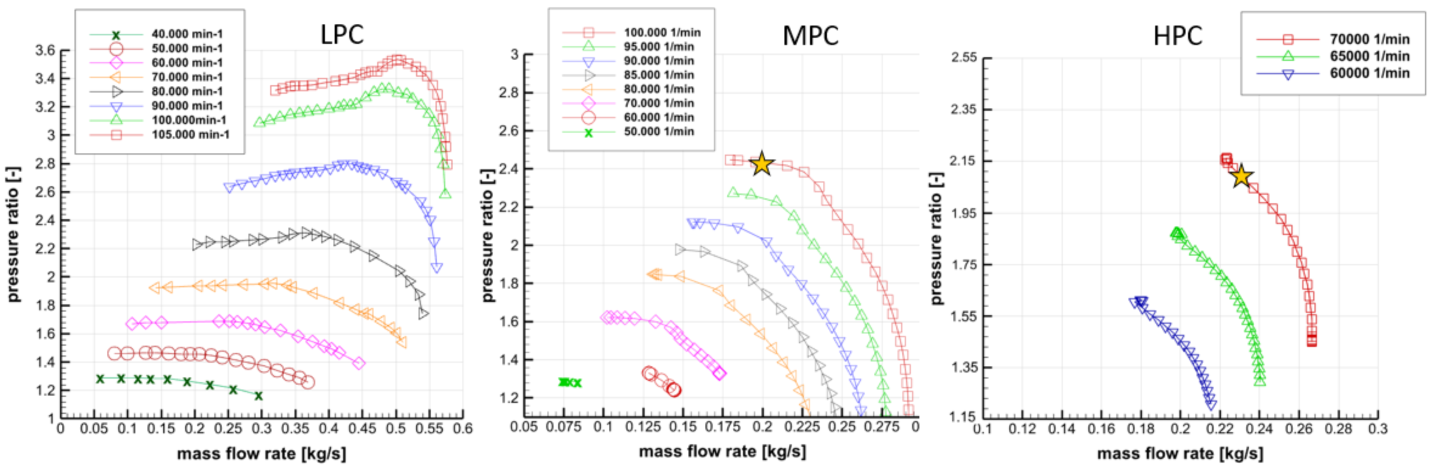

FIGURE 3: PERFORMANCE MAP OF THE LPC, MPC AND HPC

Furthermore, if it is assumed that the same compressor is always used to compress the same working medium, then equation 5 and 6 are obtained.

$$\dot{m}_{\text{red}} = \dot{m}_{\text{I}} \frac{\sqrt{\kappa_I * T_I}}{p_I * \kappa_I} = \dot{m}_{\text{II}} \frac{\sqrt{\kappa_{II} * T_{II}}}{p_{II} * \kappa_{II}} \tag{5}$$

$$n_{\text{red}} = \frac{n_I}{\sqrt{\kappa_I * T_I}} = \frac{n_{II}}{\sqrt{\kappa_{II} * T_{II}}} \tag{6}$$

On the basis of these equations, Ebsilon performs automatically the calculation for different inlet condition for a given compressor (characterized by its performance map in the design condition). Therefore, the molar mass M, the isentropic exponent κ and the design condition (pressure and temperature at the inlet of the compressor), has to be implemented. In Figure 4 the performance map of the LPC is shown.

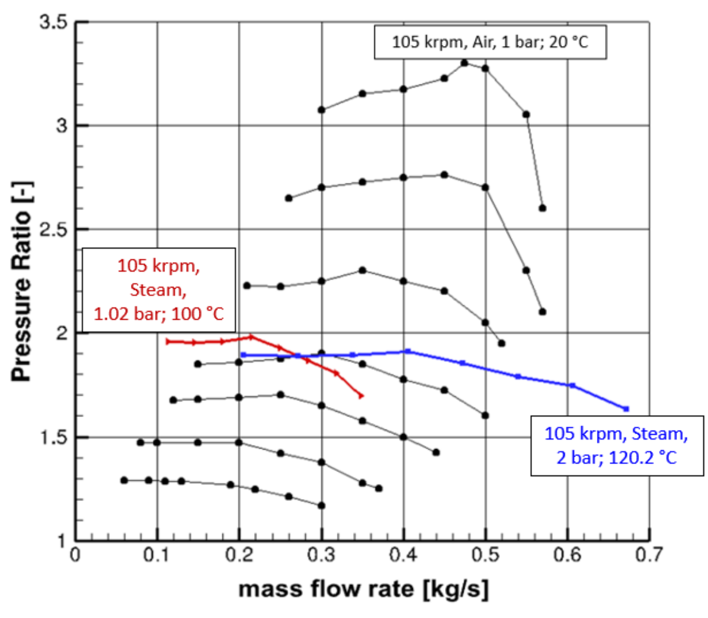

FIGURE 4: LPC PERFORMANCE MAP INCLUDING THE CONVERSION FOR OTHER INLET CONDITIONS

The black lines represent the obtained compressor speedlines measured for air under International Standard Atmosphere inlet conditions (15°C and 1013.25 hPa) Further, the red line represents the recalculated speedline of the nominal speed of the compressor (100.000 rpm black line), but instead of air the parameters for steam at 1 bar(a) and 100 °C at the inlet are used. In addition to that, the blue line shows once more the same speedline, but for the recalculation of the inlet conditions of 2 bar(a) and 120 °C are used. Based on this recalculation, the operating range of the pilot plant is evaluated.

The operating range is determined by varying three parameters in the simulation. First, the pressure ratio of each compressor is kept constant while the mass flow rate is being varied. Next, the inlet conditions, i.e. pressure and temperature in front of the LPC, are varied, see table 4. By this, the system performance can be evaluated for different applications. Furthermore, the sensitivity of the system to the compressor part-load is examined. The speed of each compressor is kept constant for a specific inlet condition within all simulation series. The relative speed remains constant for all compressors. In the final stage of the investigation, the possibility of active position adjustment of the operating point in the HPC is examined, which has a significant influence on the overall system performance. For this purpose, the superheating at the inlet is varied.

3. RESULTS AND DISCUSSION

In this section, the simulation results based in the model introduced in thre previous section, is presented. First, the design case is evaluated, which serves as a reference for the subsequent part-load operating states. The section concludes with a conceptual qualitative description of a start-up maneuver.

3.1 Design case

The design goal of the pilot plant ZiRa is to serve as a new type of HTHP with a sink temperature of at least 200 °C. The simulation results of the design case are shown in table 2. The heat pump reaches in this operational state a temperature lift of 80 K. This temperature increase corresponds to a total pressure ratio of 7.97, which includes all pressure losses through pipes, valves and

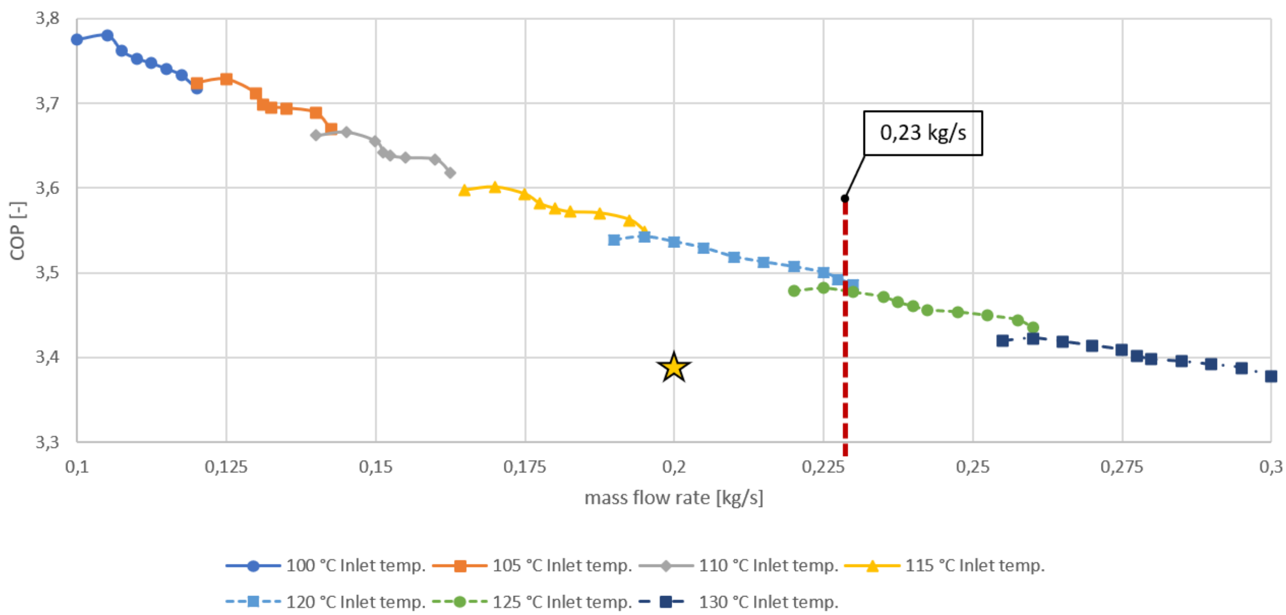

FIGURE 5: OPERATING RANGE FOR DIFFERENT INLET CONDITIONS

TABLE 2: SIMULATION RESULTS OF THE DESIGN CASE (I)

Parameter	Result
T_{Source} [°C]	120.86
T_{Sink} [°C]	200.86 (@15.833 bar(a))
COP [-]	3.39
Mass flow [kg/s]	0.2
Thermal capacity HTSC [kW]	392.98
Thermal capacity LTSC [kW]	113.14

TABLE 3: SIMULATION RESULTS OF THE DESIGN CASE (II)

Name	speed [min^{-1}]	Π [-]	η_{Comp} [%]
LPC	101300	1.9	61.8
MPC	100000	2.094	66.8
HPC	70000	2.12	64.5

the inter- and after-coolers. In principle, mass flow rates up to 0.4 kg/s can be run in the system, but since the transmittable drive power in the gearboxes of the LPC and MPC is limited to 50 kW of continuous load, a mass flow rate of 0.2 kg/s was considered. This mass flow leads to a thermal capacity of 393 kW which can be transferred from the primary cycle to the HTSC. In addition, a heat flow of 113.1 kW is transferred into the LTSC, so that the total thermal capacity is 506.1 kW.

Compared with the theoretically possible COP of 4.792 (see Equation 3), the performance of the system is comparatively good with an overall COP of 3.39 (70.742 % exergetic efficiency), although various losses have been taken into account. In this context it should be pointed out that in general it would have been possible to combine the heat flows at one temperature level. However, this consideration was discarded in the design process in order to simplify the control and increase the COP.

Table 3 shows the performance data for the three compressors. These are each operated at a respective speed close to the design point. The exception is the LPC. The LPC which is operated close to the surge limit. Due to the inlet condition, this is not possible in any other way, yet a pressure ratio of 1.9 is generated. In comparison, a pressure ratio of approximately 2.1 is possible for both, the MPC and the HPC. This shows that the compressors have been designed and optimized for the use under these inlet conditions. This can be seen in particular from the fact that both, the efficiency and the pressure ratio, are improved in comparison to the LPC.

3.2 Operating range of the pilot plant ZiRa

The part-load operating behavior for the pilot plant ZiRa is shown in Figure 5. In the simulations, different source temperatures from 100 °C to 130 °C were simulated in 5 K iteration steps. First, the minimum and maximum possible mass flow rates were determined, while neglecting the technical limitations. In order to assure comparability between the different inlet conditions, a constant pressure ratio was assumed. Therefore, the pressure ratio of the LPC was kept at a constant value of 1.9. The pressure ratio of the MPC was kept at 1.95 and the one of the HPC was kept at 2.05, respectively. The assumption of a constant temperature level in the source and sink in an industrial application is the reason for this. On this basis, the operating range of the system was determined by varying the maximum possible mass flow. This is determined by the surge or choke limit of the three compressor stages. The respective speed of a compressor can be varied. In this context, the state of superheat upstream of each compressor was kept constant at 10 K.

The operating range is visualized by the mass flow rate on

TABLE 4: TEMPERATURE LIFT FOR EACH INLET CONDITION

T_{Source} [°C]	p_{Source} [bar(a)]	T_{Sink} [°C]	T_{Lift} [°C]
100	1.0142	165	65
105	1.209	172.5	67.5
110	1.4338	180	70
115	1.6917	187.5	72.5
120	1.9866	195	75
125	2.3222	202.5	77.5
130	2.7025	210	80

the $x-$axis and the COP on the $y-$axis as an evaluation criterion. The highest COPs are achieved at the lowest temperature lift. For this reason, there is a nearly linear decrease in the COP values, since the maximum pressure and thus the possible temperature lift increases linearly with inlet pressure. This relationship is particularly evident at the data point with an inlet temperature of 120 °C and a mass flow rate of 0.2 kg/s, as these are the boundary conditions of the design case (depicted by the yellow star in Figure 3). The maximum available temperature lift is not achieved when compared to the the design case. The temperature lift is 5 K lower which causes the COP value to be higher by 4.3 %.

As described earlier, a continuous load of 50 kW can be transmitted via the gearboxes of the LPC and the MPC. This technical limit is represented by the red dotted line in Figure 5. Generally, it would be possible to cover a wider operating range with the applied compressors, but this would require further adjustments to the gearboxes.

Basically, an almost horizontal line of the COP would be expected with nearly constant inlet conditions over the operating range. Figure 6 shows an example of the COP value for the design inlet conditions (1.987 bar(a) and 120 °C). It can be seen that the COP values (blue line - corresponding to the left $y-$axis) decrease with increasing mass flow rate. This is due to the change in the impeller efficiencies. The peak is reached at the mass flow rate of 0.195 kg/s. At this operating point, the MPC and the HPC are operated close to the maximum efficiency. In addition, it can be seen that the efficiency of the LPC increases with the increment in the mass flow rate as the distance to the surge line increases (see in Figure 3). Hence, the operating point within the performance map is closer to the optimum. In general, an increase in the mass flow rate leads to a deterioration of the MPC and HPC efficiencies by 2 % and 3.7 % respectively, which is why the overall COP decreases. This change in conditions cannot be compensated by the increase of approximately 3% in LPC efficiency.

3.3 Part load operation

In the following section, the part-load operation is considered at a constant temperature of 120 °C (@1.987 bar(a)) at the inlet of the LPC. Based on the results of the previous section, a variation of the mass flow rate was carried out in addition to the speed variation. In the simulations, a constant relative speed was assumed for all three compressor stages.In this context, 100 % relative speed corresponds to the values given in table 3. In Figure 7 the obtained pressure values at the outlet of the HPC

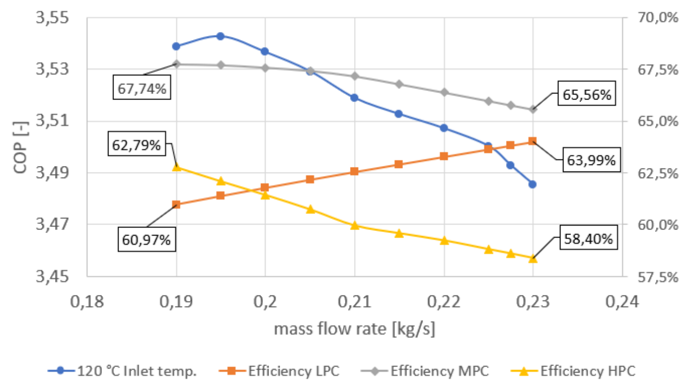

FIGURE 6: IMPACT OF THE COMPRESSOR EFFICIENCY ON THE SYSTEM PERFORMANCE

are shown as a function of the relative speed. With the minimum mass flow rate, a decrease in outlet pressure downstream of the HPC of 17.51 % was achieved by decreasing the speed by 2.5 %. With a mass flow rate of 0.205 kg/s a decrease of 19.95 % of the outlet pressure results with same decrement of the relative speed. The maximum reduction in the considered operating range occurs at the highest mass flow rate. The decrease was calculated to a value of 24.93 %. These observations reveal that the pilot plant is susceptible to small changes in the inlet coniditons.

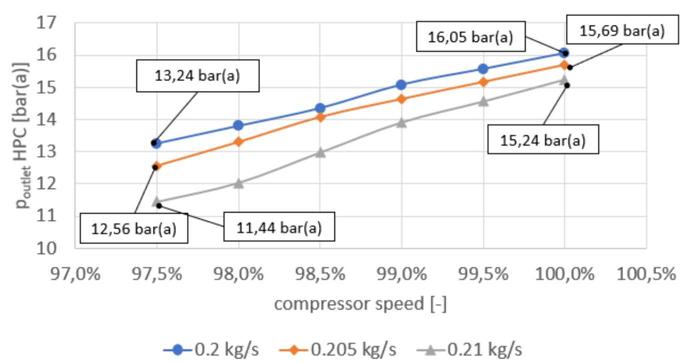

FIGURE 7: DEPENDENCY OF THE OVERALL PRESSURE BASED ON DIFFERENT COMPRESSOR SPEEDS

This significant decrease in the pressure ratio is not not only caused by the decrease in speed, but also by the change of inlet conditions. Due to the latter, also a deterioration is caused in efficiency. Figure 8 shows the change in the pressure ratio for the respective speed of each compressor (for better visibility, only three operating points are shown for the LPC and MPC.). This clearly shows how strongly the part-load conditions decrease for each stage. In the illustration, the pressure ratios were recalculated for the MPC and HPC to the CFD map value (factor 0.85 as described in section 2). Therefore, the achievable pressure ratios in the stationary simulation are lower. However, the change in relative speed from 100 % to 97.5 % and pressure ratio decreases associated with it remain the same. It can be seen that the pressure ratios in the LPC and in the MPC change slightly.

With the LPC, the pressure ratio change is 2.2 % between

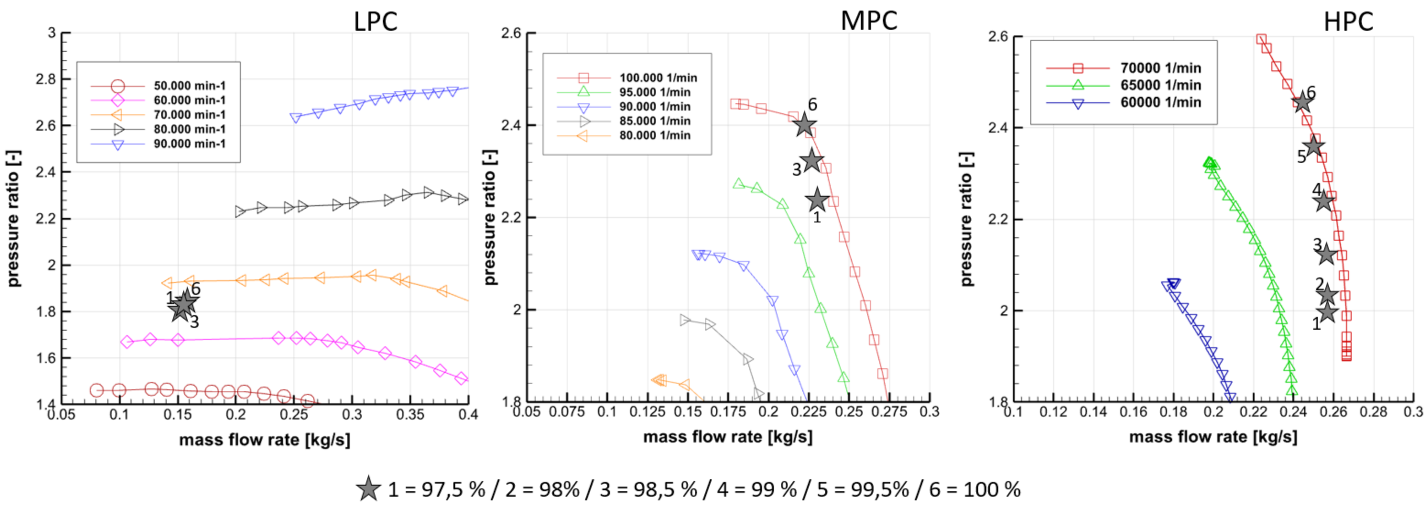

FIGURE 8: OPERATING POINTS FOR SIX DIFFERENT SPEED VALUES FOR EACH COMPRESSOR VISUALIZED BY A STAR

the relative speed of 97.5 % and 100 %. Although the change in the MPC increases by nearly 2 % to 4.1 %, the change takes full effect in the HPC mainly. At a relative speed of 97.5 %, the HPC can operate at highly throttled conditions only, so that a pressure ratio of 1.7 is achieved. Figure 8 shows this for the considered case of a mass flow rate of 0.21 kg/s. The relative change in the pressure ratio is then 18.1 %.

3.4 Impact of the degree of superheating

The superheating is investigated as an option for increasing the performance of the pilot plant. This enables the operating point of the respective compressor to be shifted towards a more efficient operating point. Based on the results in the previous section it can be seen that a wide operation range is necessary, especially for the high-pressure compressor. For this reason, the investigation of the influence of the superheat for increasing the performance of the system was carried out for the HPC. It was assumed that the biggest impact of the superheating will be in part-load. Therefore, the mass flow rate was set to 0.21 kg/s and the operating speed of each compressor was set to 98 % of the nominal speed.

In Figure 9 four different operating points are displayed, which represent four degrees of superheating (5, 10, 15 und 20 K). Compared to the design case (10 K), the pressure ratio can be increased by 3 % and the efficiency by 1.35 % assuming the degree of superheating is to be decreased to 5 K. The reduction in superheat leads to an increased pressure ratio at the same reduced speed (see equation 6). Assuming a constant mass flow rate, this results in its comparatively better position of the operating point in the compressor map. Hence, the distance to the choke line is increased, which in turn increases the impeller efficiency. As a consequence, the overall performance of the system can thus be improved. The simulation with a superheat of 15 and 20 K, on the other hand, shows a deterioration in the performance. This is due to the shift towards the choke limit, which reduces the impeller efficiency. Furthermore, the required power input is increased due to the elevated inlet temperature. Based on the results described above, it can be concluded that

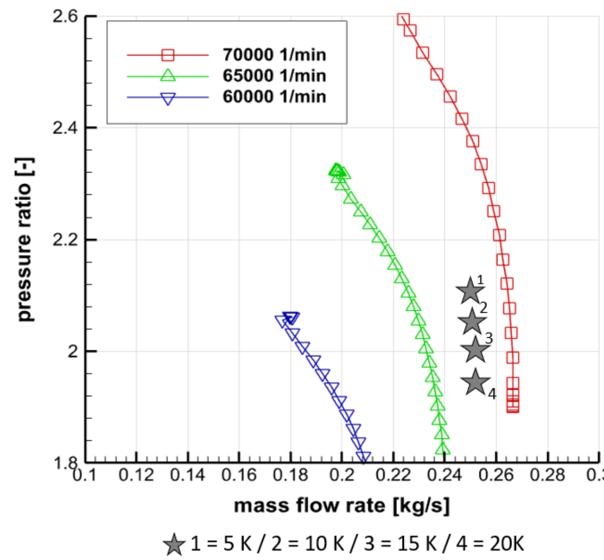

FIGURE 9: OPERATING POINT OF THE HPC DEPENDENT ON THE DEGREE OF SUPERHEATING VISUALIZED BY A STAR

for the presented operating condition a reduction of superheating can be an adequate means of improving the overall system performance. Since the investigation presented here evaluates a single operating point, this assessment may lose its validity, especially at other part-load operating points. For this reason, it is advisable to carry out a separate examination of each operating point prior to future tests of the pilot plant.

3.5 Start up procedure

The plant start-up procedure begins with all sections being preheated, which means that hot water respectively water vapor is circulating through the plant until a steady-state condition is reached. First, the HTSC is put into operation. Therefore, the electric heater is used. This process is completed as soon as a constant temperature of 120 °C (in the design case) is reached in

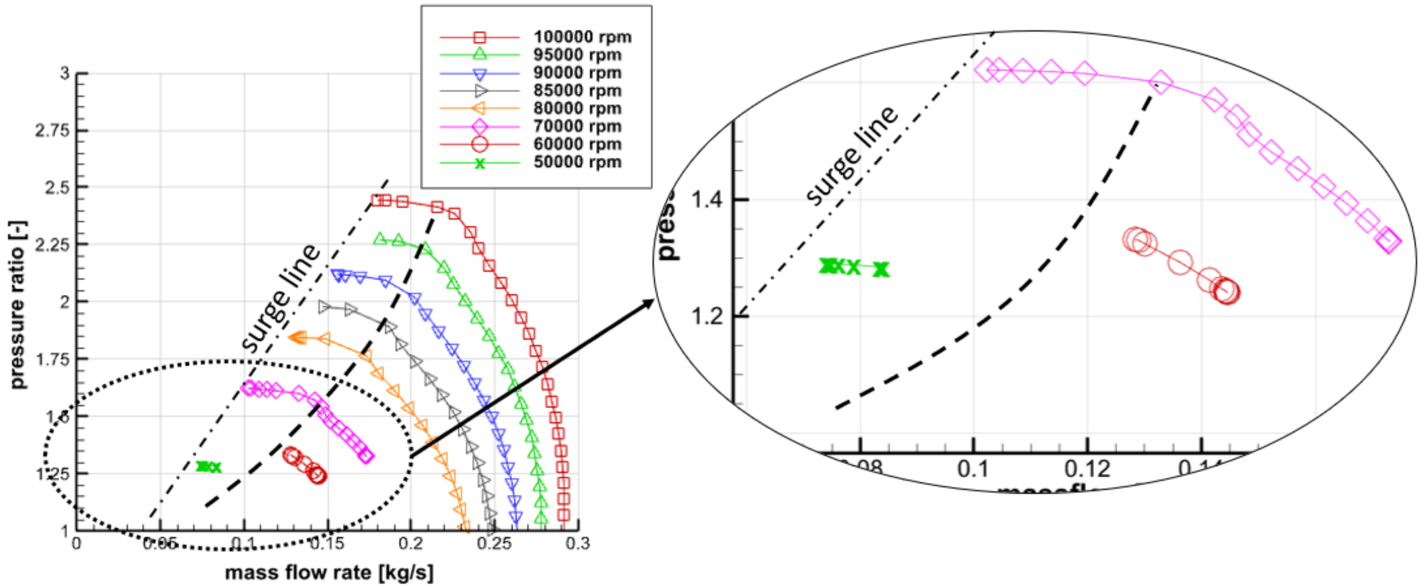

FIGURE 10: PERFORMANCE MAP OF MEDIUM PRESSURE COMPRESSOR WITH DETAILED SECTION

the evaporator. During this process the continuous evaporation of the water vapor in the primary cycle starts. At the beginning, the air must be removed from the primary cycle. Therefore, the water vapor mass flow is withhold by a shut-off valve in the evaporator until an operating pressure of approximatley 2 bar(a) is reached. Next, this valve will be opened and the water vapor forces the air out of the system. By a continuous mass flow rate the primary cycle is heated up. In the process, the compressors are initially left out via a by-pass. As soon as a stationary temperature profile is reached in the entire primary cycle, i.e. a temperature of 120 °C with respect to the design case, the start-up process of the compressors begins. During start-up, the operating range of the respective compressor, including its natural frequencies and its maximum temperature gradient, must be taken into account. The compressors are started up in the following order: LPC, MPC and HPC. Finally, the LTSC is heated using the heat generated by the compression process. Compressor speeds of up to 100,000 rpm require a detailed consideration of the dynamic behavior in order to ensure safe system operation. The knowledge of the natural frequencies with the corresponding natural modes of vibration is of particular importance. If the excitation frequencies and modes largely coincide with natural frequencies and modes, the state of resonance occurs. This state of resonance must be avoided in order to rule out damage to the compressor. During the design process, rotordynamic calculations of the shaft with impeller and bearing of the respective stage are first carried out in order to show critical operating points. In case a safe operation is not possible from a rotordynamic point of view, an adjustment of the design can be made in the design phase. In the next step, the installation of the respective compressor stage is designed from a structural-dynamics point of view and checked by experimental investigations after assembly. This is done by a modal analysis on the real object. If the resonance ranges cannot be avoided by design, the corresponding speed bands are blocked for operation. The start-up of the compressors is described in the example using the medium-pressure compressor. As described, this is based on the performance maps, see Figure 10. This shows an inhomogeneous picture, especially at the lower speed ranges. While at 50.000 min^{-1} the surge line can be mapped according to the speedlines 70.000 min^{-1} and higher, this is not possible at 60.000 min^{-1}. In contrast, this has a correspondingly mapped surge limit, compared to the other speedlines. For this reason, it is currently assumed that the convergence problem of the numerical flow simulation does not correspond to reality and therefore, stable operating conditions can be approached. The medium-pressure compressor is first accelerated to a minimum speed of 30.000 min^{-1}, which is necessary for the seal to function. At this speed, the compressor train is warmed up. The speed is subsequently increased in intervals. A stationary temperature downstream of the compressor is assumed as the evaluation standard. The back pressure of the compressor can be evaluated in each case from the amount of steam removed into the condenser, which is controlled via the secondary-side flow.

4. CONCLUSION

Alongside of the latest concept of the pilot plant ZiRa the steady-state simulation model, used for the design of the ZiRa was presented. Based on this model, the operating range was investigated, in particular on the basis of the compressor characteristics. The change in COP for different source temperatures was shown. It has been presented that the respective operating point within each compressor performance map is decisive for the performance of the system. Hence, there is a direct proportionality of the compressor efficiencies to the COP. Furthermore, the performance of the pilot plant at compressor part-load operation was presented. The simulation results revealed a significant dependency of the performance on small changes in the inlet conditions. In general, the available maximum temperature and pressure conditions correlate strongly with the respective compressor operating point. For this reason, it was also investigated to what extent it is possible to influence the inlet conditions by varying the degree of superheating. In the selected example an improvement in performance was achieved by lowering the degree of superheating. However, this cannot be generalized. Based on these results, an individual compressor development is considered to be of limited value. If there are sufficient resources available, a serial optimization of the three compressors should be carried out within one CFD setup, taking part-load operating conditions into account. In this context, a redesign of the HPC will be carried out in order to significantly extend the operating range.The results presented in this paper represent the steady-state operation of the plant only. These must be extended to include transient simulations to determine the time-dependent temperature influences and the heat transfer during the start-up of the system. In addition, a detailed validation of the simulation results must be carried out by measurement campaigns. This includes in particular the acquisition of the compressor performance maps for both fluids, air and water vapor. The results are used to determine the correlation between these different working media and to establish a comparison between experiment and simulation.

ACKNOWLEDGMENTS

This work wouldn't be possible without all the hard work of every member of the department of high temperature heat pumps while design and construction of the Pilot ZiRa. The author would like to thank every one of them for their dedication and their continuous, patient work.

REFERENCES

[1] Adamson, K.-M., and Sjolander, S. A., 2022. "High-temperature and transcritical heat pump cycles and advancements:a review". *Renewable and Sustainable Energy Reviews 167*.

[2] Arpagaus, C., 2018. "High temperature heat pumps: Market overview, state of the art, research status, refrigerants and application potentials". *International Refrigeration and Air Conditioning*.

[3] Marina, A., 2021. "An estimation of the european industrial heat pump market potential". *Renewable and Sustainable Energy Reviews*.

[4] de Boer, R., 2020. "Industrial heat pump whitepaper".

[5] Oehler, J., 2020. "Part load capability of a high temperature heat pump with reversed brayton cycle". *Proceedings of the 13th IEA Heat Pump Conference*.

[6] Oehler, J., 2022. "Simulation of a safe start-up maneuver for a brayton heat pump". *Proceedings of the ASME 2022 International Mechanical Engineering Congress and Exposition*.

[7] Schiffmann, J., and Favrat, D., 2009. "Experimental investigation of a direct driven radial compressor for domestic heat pumps". *International Journal of Refrigeration,* ***32***(8), pp. 1918–1928.

[8] Zuehlsdorf, B., 2019. "Analysis of technologies and potentials for heat pump-based process heat supply above 150°c". *Energy Conversaion and Management: X*.

[9] Šarevski, M. N., and Šarevski, V. N., 2017. "Thermal characteristics of high-temperature r718 heat pumps with turbo compressor thermal vapor recompression". *Applied Thermal Engineering,* ***117***, pp. 355–365.

[10] Šarevski, M., and Šarevski, V., 2012. "Characteristics of water vapor turbocompressors applied in refrigeration and heat pump systems". *International Journal of Refrigeration,* ***35***(5), pp. 1484–1496.

[11] Meroni, A., 2018. "Design of centrifugal compressors for heat pump systems". *Applied Energy 232*.

[12] Schaffrath, R., 2022. "Multi operating point aerodynamic optimization of a radial compressor impeller for an application in high temperature heat pump". *Proceedings of the ASME 2022 International Mechanical Engineering Congress and Exposition*.

[13] Zuehlsdorf, B., 2018. "Recommendations for r-718 heat pumps in high temperature applications". *Proceedings of the 13th IIR-Gustav Lorentzen Conference on Natural Refrigerants*.

[14] Steag Ebsilon. URL: https://www.ebsilon.com/de/, Accessed 18.12.2022.

[15] International Association for the Properties of Water and Steam. URL: http://www.iapws.org/newform.html., Accessed 20.12.2022.

[16] Scholz, G., 2013. *Heisswasser- und Hochdruckdampfanlagen*. Springer Vieweg.

[17] Bräunling, W., 2015. *Flugzeugtriebwerke*. Springer Vieweg.

[18] Roberts, S. K., and Sjolander, S. A., 2002. "Effect of the specific heat ratio on the aerodynamic performance of turbomachinery". *Journal of Engineering for Gas Turbines and Power*.